Advances in Artificial Intelligence and Machine Learning; Research 5 (1) 3476-3494 Received 16-12-2024; Accepted 20-03-2025; Published 27-03-2025

Framework to Detect COVID-19 from Chest X-Ray/CT using Deep-Learning and Arithmetic-Optimization Algorithm

Fadiyah Almutairi fma.almutairi@mu.edu.sa
National Department of Computer Engineering,
College of Computer and Information Sciences,
Majmaah University, Majmaah,11952,
Saudi Arabia

Corresponding Author: Fadiyah Almutairi

Abstract

The lung infection caused by COVID-19 constitutes a medical emergency, necessitating prompt detection and treatment to mitigate its effects. Clinical diagnosis and assessment of severity are typically conducted utilizing medical imaging practices, like chest X-rays and lung CT scans. Owing to its advantages, Deep-Learning (DL) frameworks are extensively developed to identify occurrences utilizing clinically obtained X-ray/CT data. This study plans to propose a novel framework for COVID-19 detection in X-ray/CT images utilizing the Lightweight Deep-Learning Model (LDLM). This framework included the LDLM features alongside the Local Binary Pattern (LBP) features to enhance detection efficacy. Additionally, to reduce the over-fitting problem, this framework utilized the Arithmetic-Optimization Algorithm (AA) for features reduction and fusion to enhance detection accuracy. The stages of this framework encompass; data collecting and preliminary adjustment, feature extraction utilizing LDLM, and LBP, feature selection by AA and serial feature concatenation, and classification employing five-fold cross-validation. The suggested framework was evaluated and validated using the benchmark image database, yielding accuracy >99% for both X-ray and CT based examinations. These results validate that the proposed approach yields substantial outcomes on the selected benchmark database.

Keywords: Lung infection, COVID-19, Deep learning, Machine learning, Arithmetic-optimization algorithm, Detection.

1. INTRODUCTION

The lung is a vital organ in human physiology, and diseases affecting the lung can lead to significant health complications. The recent worldwide outbreak of the coronavirus disease (COVID-19) has presented an unprecedented challenge to the global healthcare system. This illness mostly impacts the lungs and induces respiratory complications ranging from moderate to severe. COVID-19 is a contagious disease that transmits from infected persons to healthy ones. The disease will disseminate widely among individuals due to its swift transmission rate. Moreover, its potential for catastrophic effects has underscored the urgent detection and adequate management of COVID-19

Citation: Fadiyah Almutairi. Framework to Detect COVID-19 from Chest X-Ray/CT using Deep-Learning and Arithmetic-Optimization Algorithm. Advances in Artificial Intelligence and Machine Learning. 2025;5(1):199.

as a critical concern. Accurate identification of COVID-19 is crucial for mitigating its transmission and enhancing patient outcomes [1, 2].

Previous studies on COVID-19 confirm that medical imaging practices, including chest X-rays and computed-tomography (CT) slices, are standard procedures for diagnosing and evaluating lung infections [3–5]. These imaging modalities present a complete observation of the pulmonary alterations associated with the disease, including ground-glass opacities, consolidation, and other distinctive patterns. The preliminary evaluation of COVID-19 by Reverse Transcription-Polymerase Chain Reaction (RT-PCR) is the definitive standard for verifying the infection. The RT-PCR test has limitations such as limited availability, delayed results, and variable sensitivity. The availability of medical imaging modalities, like X-ray/CT, has arisen as an auxiliary investigative tool when the patient's condition is severe and does not necessitate RT-PCR confirmation [6, 7].

Recent advancements in artificial intelligence (AI) and deep learning (DL) have enhanced illness diagnosis through medical imaging techniques [8, 9]. These technologies facilitate the automation of disease assessment using selected imaging modalities, hence enhancing diagnostic accuracy. Deep learning frameworks have demonstrated exceptional proficiency in interpreting intricate medical imaging. These frameworks have been extensively utilized for COVID-19 identification through X-ray and CT imaging, and the results are deemed essential for the design and implementation of requisite treatment [10].

Despite the existence of enhanced deep learning methods in the literature, challenges such as overfitting, computational complexity, and the requirement for extensive annotated datasets persist in the development and implementation of suitable deep learning schemes. Proposing a deep learning solution to address the aforementioned difficulties remains a formidable challenge. Recent methodologies, such as the modified DL-scheme, heuristic-based feature optimization, and ensemble techniques, are effective in mitigating difficulties related to overfitting and complexity [11].

Numerous deep learning algorithms have been developed to recognize COVID-19 utilizing X-ray and CT images, owing to their clinical significance and enhanced accuracy. The previous studies introduced several traditional and Lightweight Deep Learning Models (LDLM) for the recognition of COVID-19 from the selected imaging modality [12–14]. In contrast to the traditional deep learning approach, the LDLM features a less sophisticated architecture, facilitating easier parameter adjustment for the selected images. This study employed the LDLM framework for the identification of COVID-19 in selected lung pictures. This LDLM structure integrates the efficacy of lightweight architectures with contemporary feature selection methods to deliver a scalable and effective solution for practical clinical image analysis tasks.

This framework amalgamates deep features with handmade features to augment detection efficacy. Additionally, to enhance accuracy, it employed heuristic-algorithm-based optimization for feature selection and serial feature production. This project seeks to construct a deep learning framework to enhance the recognition of COVID-19 in X-ray/CT with increased accuracy.

This tool comprises the following phases: X-ray/CT collection and resizing to 224x224 pixels, deep feature extraction utilizing the selected LDLM, conventional feature extraction employing LBP, feature optimization via the Arithmetic-Optimization Algorithm (AA), concatenation of serial features to obtain the fused features (FF) vector, and classification with five-fold cross-validation. The COVID-19 detection process is initially conducted utilizing LDLM features with the SoftMax

classifier, confirming that MobileNetV1 (MNV1) and NASNetLarge (NNL) yield superior detection accuracy for both X-ray and CT databases. The created system evaluated the following features to verify the merit of the selected image databases. Following the optimization of the LDLM and LBP features through AA, the subsequent feature vectors are constructed to evaluate the efficacy of the developed framework: (i) serial concatenation of MNV1 and NNL (FF1), (ii) serial concatenation of MNV1 and LBP (FF2), (iii) serial concatenation of NNL and LBP (FF3), and (iv) serial concatenation of MNV1, NNL, and NNL (FF4).

The investigational results of this research demonstrate a detection accuracy of 99% for both X-ray and CT images utilizing FF4 and K-Nearest Neighbour (KNN) classification methods. This study established a distinctive framework that is effective for both X-ray and CT pictures. The results of this investigation validate that the suggested technique yielded a clinically significant outcome for COVID-19 identification, and in the future, this framework may be utilized to analyze actual clinical lung pictures obtained from infected patients.

The contributions of this study include;

i Development of a unique framework for COVID-19 detection from X-ray/CT images.

ii Implementing AA-based feature selection to reduce overfitting issue,

iii Improving the detection accuracy using the LDLM and LBP features.

Remaining part of work is organised as follows; Section 2 shows literature review, Section 3 depicts methodology, and Sections 4 and 5 shows the result and conclusion.

2. LITERATURE REVIEW

DL-based schemes are widely considered in medical image examination tasks due to its better accuracy and reliability. These methods help to provide a significant result on the chosen disease, which was then considered by the doctors for decision making and treatment planning tasks. The recent advancements and the implementation easiness helped to adopt the DL-based approaches in real clinical data examination tasks [15].

The literature confirms that the implementation of the DL-techniques is commonly considered for COVID-19 detection using chosen lung image database. The imaging modalities, like chest X-ray/CT images are common tools for detecting the presence of lung infection and its severity. Hence, most of the earlier works considered the DL-methods for analyzing these images [16, 17]. Compared to the conventional schemes, the LDLM have simple and effective architecture and hence, most of the COVID-19 detection approaches considered these models to examine disease in X-ray/CT slices. Summary of few selected procedures are presented in TABLE 1.

TABLE 1 provides the information about some chosen image examination methods with DL-models. Most of these methods considered the X-ray/CT images to identify the lung infection. In real clinical cases, implementing and executing separate DL-model is easy and the chosen model helps to detect the COVID-19 disease from either X-ray or CT. The availability of unique model which help to analyse both image modality is less in the literature. The recent work of Appavu et al. (2024)

Table 1: Summary of DL-based COVID-19 detection from X-ray/CT images

Reference	Examination procedure
Hussain, et al. (2021) [18]	This study introduced an innovative COVID-19 recognition technique utilizing an X-ray database, achieving an accuracy of 99.1% in binary classification.
Jain, et al. (2021) [19]	A standard DL-model-based technique was implemented to analyze the X-ray database, accomplished an accuracy of 97.97%.
Ozturk, et al. (2020) [20]	DL-models were implemented to distinguish the COVID-19 disease in X-ray, and the accuracy of the detection was 98.08%.
Ayalew, et al. (2023) [21]	This work proposed a convention DL-model based X-ray examination and achieved a training accuracy of 99.8% and testing accuracy of 99.1%.
Ulutas, et al. (2023) [22]	Development of a novel scheme; CovidxNet-CT is discussed and achieved an accuracy of 98.83% with the chosen CT database.
Gupta and Bajaj (2023) [23]	This work proposed a LDLM based COvid-19 detection and achieved 98.91% when CT slices are considered.
Arshad, et al. (2023) [24]	This work proposed DL-based detection of COVID-19 in lung CT slices and achieved 99.5% accuracy when Resnet101 is considered.
Duong, et al. (2023) [25]	This work executed the DL-based examination on the large image database of X-ray and CT and obtained 95% accuracy.
Choua, et al. (2022) [26]	This work presented a framework for X-ray and CT image analysis and the VGG19 based detection provided an accuracy of 90.3%.
Xue, et al. (2023) [27]	Proposing a DL-framework for disease detection in X-ray and CT is presents and this work achieved accuracy up to 99%.
Shyni and Chitra (2022) [28]	This research implemented the DL-model based COVID-19 detection approach using X-ray and CT and achieved 99.18% accuracy with MNV1 model.
Maghdid, et al. (2021) [29]	This work proposed a DL-based COVID-19detection using X-ray and CT is presented and this work achieved an accuracy of 98%.

proposed a unique DL-framework using conventional VGG16 scheme and achieved a detection accuracy of 99.58% with X-ray and 94.29% with CT-scan slices [30]. Compared to the X-ray, the detection accuracy achieved with the CT is considerably less. Further, the earlier work was implemented using the conventional model, which is having a larger parameters compared to the LDLM.

This work presented a framework utilizing the LDLM to enhance detection accuracy relative to the previous study in [31] for both X-ray and CT images. This research examined LDLM- and LBP-features to develop the framework. Additionally, it evaluated AA-based feature selection and the concatenation of serial features to combine optimized LDLM and LBP features, therefore enhancing detection accuracy for both X-ray and CT images. The findings of this study validate that this technique achieves an accuracy exceeding 99% for lung image cases. These results indicate that the technique yields significant outcomes on the selected database, and its clinical relevance may be substantiated in the future through the analysis of clinically obtained lung images of COVID-19 patients.

3. METHODOLOGY

The performance of the automatic disease detection based on the chosen medieval imaging scheme depends on the data and employed technique. Every DL-technique needs a specific data dimension and hence, each image to be examined to be resized before it is to be analysed with the chosen scheme. This part of the study presents the proposed framework to employ to effectively analyse the chosen lung images.

3.1 Developed Framework

This sub-section of the work presents the framework developed to distinguish COVID-19 from X-ray/CT data. This framework consist the two major sections, such as the image examination based on the achieved features and performance evaluation and confirmation using the chosen metrics.

Different stages of this framework are as follows; when a patient is admitted in hospital with lung infection due to COVID-19, initially the RT-PCR test is recommended to confirm the disease. The RT-PCR test is a time consuming process and the next stage of the examination needs to be executed based on the patient's health condition. When the patient condition is abnormal, then without the RT-PCR, the lung examination based on X-ray/CT is recommended. During this process, the patient preparation and image based analysis will be performed in a controlled environment. After collecting the image using a chosen scheme, it is then verified by the doctor to confirm about the disease and its severity. Based on the observation by the doctor, the necessary treatment will be executed to reduce the severity of lung infection. The recent medical images are digital in nature. After the verification of the images by the doctor, these images are then processed (initial image adjustment and labeling) using a recommended technique. The processed images are then stored in the chosen digital repository for future examination purpose.

In this research, the digital lung images (X-ray/CT) available in [32] are considered for the examination. Every collected image is resized to 224x224 pixels and then considered for the examination. The processed images from the data repository are considered for the feature extraction with LDLM and LBP. This procedure helped to obtain 1x1x1000 deep-features from the chosen model and 1x1x59 LBP features. The chosen LBP is executed using different weights (W=4) and hence, the total LBP features during this process is about 1x1x236. Integration of the LDLM and LBP features may provide a huge feature vector which may initiate the overfitting issue. Hence, these features are reduced using the AA and then serially concatenated to get a new fused-features (FF) vector. This FF is then considered to detect the COVID-19 using the chosen classifier and the outcome if verified using 5-fold cross-validation. The result of this process provides a CM, and the necessary values, like the TP, FN, TN, and FP are then considered to compute the final metrics, like ACC, PRE, SEN, SPE, and F1S as in FIGURE 1. Based on these values, the merit of the developed framework is confirmed using the X-ray and CT images.

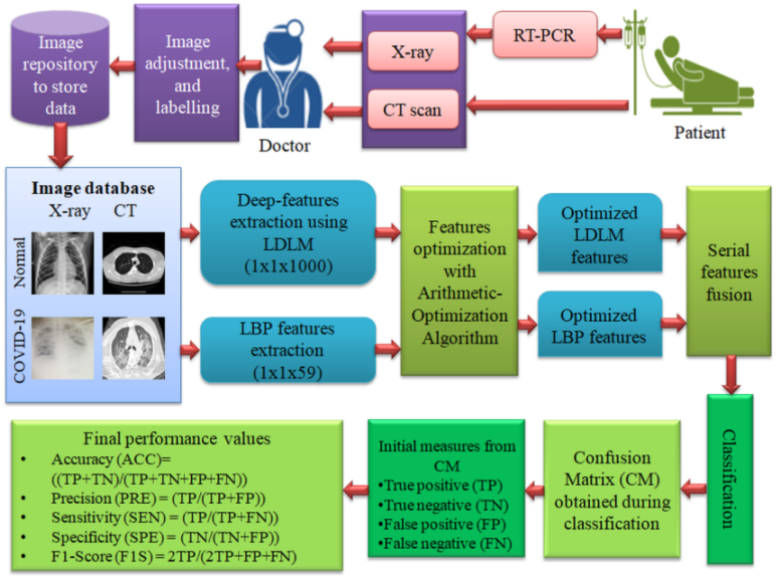

Figure 1: Proposed unique COVID-19 detection framework

3.2 Lung Image Database

In medical image examination with DL-based tool, it is essential to use clinical images to verify the performance of developed system on the clinical-data, in future. This work considered the benchmark normal/COVID-19 images available in [32]. This database consist the labeled images of X-ray and CT collected and stored in the data repository for further investigation.

3.2.1 Chest X-ray

The chosen database consist the labeled images of X-ray for verifying the performance of the developed DL-tool. In this database, 3794 numbers of X-ray images are labeled as COVID-19 class and 5500 images are labeled as normal class. To have a balanced image in every category, this work considered only 3790 images per class for the investigation after resizing it to 224x224 pixels. FIGURE 2 depicts the sample images available in the chosen database and TABLE 2, depicts the necessary information about the total, images to train the chosen DL-model and images used to test the performance.

Table 2: Number of X-ray images used in developed framework

Class	**X-ray images**			
	Total	**Train**	**Validate**	**Test**
Normal	3790	3032	379	379
COVID-19	3790	3032	379	379

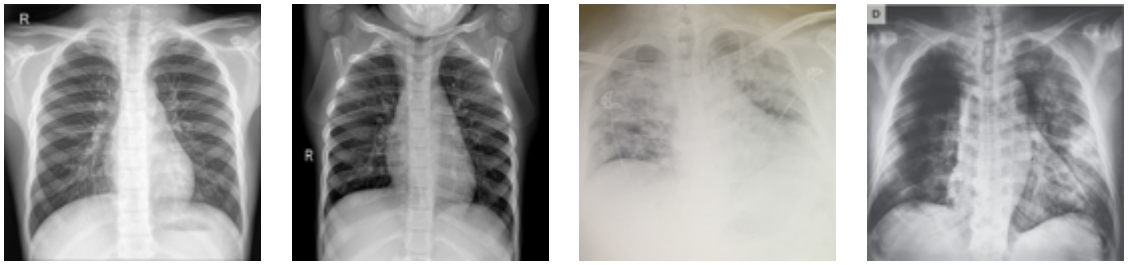

(a) Normal (b) COVID-19

Figure 2: Sample X-ray images of 224x224 pixels from the chosen image database

3.2.2 Lung CT slice

The selected CT database comprises labeled images for assessing the efficacy of the created deep learning technique. This database contains 5,426 CT slices grouped as COVID-19 and 2,628 images classified as normal. This study utilized 2,620 images per category, resized to 224x224 pixels, to provide a balanced representation across all classes. FIGURE 3 illustrates the example images from the selected database, while TABLE 3, presents the essential information about the total number of images for training the chosen DL-model and the images utilized to assess the effectiveness of this scheme.

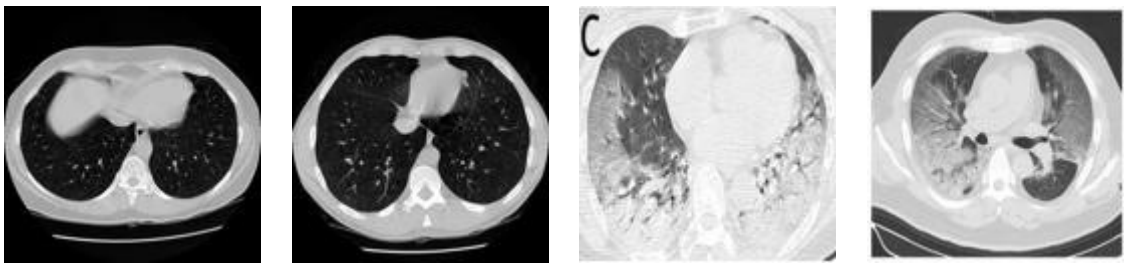

(a) Normal (b) COVID-19

Figure 3: Sample CT slices of 224x224 pixels from the chosen image database

Table 3: Number of CT slices images used in developed framework

Class	**CT slices**			
	Total	**Train**	**Validate**	**Test**
Normal	2620	2096	262	262
COVID-19	2620	2096	262	262

3.3 Lightweight Deep-Learning Scheme

The computer algorithm based data examination is commonly adopted practice in COVID-19 detection and the outcome helps to provide the information about the disease and its severity. Recently

DL-based methods are widely considered to examine the X-ray/CT images. The conventional DL-models help to provide improved recognition results on the chosen image data. Due to its large parameters, these models have computation complexity and hence, most of the recent works considered the LDLM to develop the disease examination tools [33].

This work considered the LDLM models, like the MNV1, MobileNetV2 (MNV2), MobileNetV3Small (MNV3S), MobileNetV3Large (MNV3L), NASNetMobile (NNM), NNL, and SqueezeNet (SN) for the investigation [34]. These models are assigned with the following initial values; learning rate= 1e-5, chosen performance metrics to guide the training= accuracy and loss, batch size= 16, pooling= max, optimizer= Adam, activation=ReLU, and classifier= SoftMax (SM). In this work, the number of epochs for training the LDLM is chosen as 150. The initial classification is performed using the SM with 5-fold cross-validation and the best outcome among the 5-fold is preferred as final result by the model.

3.4 Local Binary Pattern Features

Image based examination of Normal/COVID-19 class is commonly performed by analysing the image patterns in both X-ray and CT. Most of the recent works confirms that the LBP features helps to achieved better detection accuracy when it is considered for the image examination task. The necessary information about the LBP can be found in following work [35]. Earlier research which considered the LBP features can be found in [36].

This work considered the examination of the chosen images using LBP with varied weight as discussed in [36]. The weight (W) for these patterns is chosen from 1 to 4 and every image provides the LBP patter of size 1x1x59. Hence, the total features obtained for W=4 is around 1x1x236. These features are also recorded as .CSV file for future examination task using the chosen AA. FIGURE 4 presents the LBP obtained for a sample COVID-19 class X-ray and CT image. FIGURE 4(a) – FIGURE 4(d) shows the outcome for W1 to W4, respectively.

3.5 Arithmetic-Optimization Algorithm

Heuristic algorithm based feature optimization is widely adopted in various machine-learning and DL-based data examination tasks to avoid issue of overfitting. The earlier works in the literature adopted various heuristic algorithm to optimize the features in the chosen task and this technique helped to provide a better detection results during image based disease examination task. This work considered the AA-based feature selection to optimize the chosen LDLM- and LBP-features and the reduced features are then serially concatenated to get the fused-features (FF) vector. The chief reason for selecting the AA for this research is, it considers the simple mathematical practice prime part during the algorithm updating process. The AA algorithm agent movement is guided by this process, which helps to identify the optimal result when the number of iteration of the algorithm increases. Similar procedure is adopted during the feature selection task between the normal and COVID-19 classes and hence, this research considered the fireflies as the best feature selection agent.

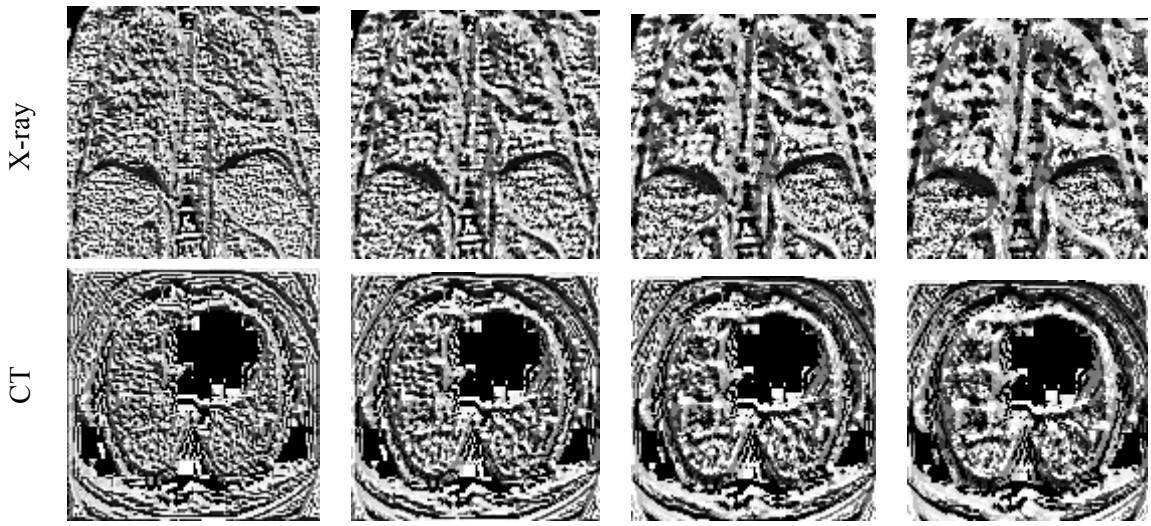

(a) W1 (b) W2 (c) W3 (d) W4

Figure 4: LBP patterns of a chosen X-ray/CT image for various weights

The AOA is initially proposed by Abualigah et al. in 2021 [37] using the conventional mathematical operations, like addition, subtraction, multiplication, and division. The mathematical description of AOA is described in Eqns. (1) to (5) [38];

Let the initial values of the agents (x) are as follows;

$$\begin{bmatrix} x_{1,1} & \cdots & x_{1,n} \\ \vdots & \ddots & \vdots \\ x_{N,1} & \cdots & x_{N,n} \end{bmatrix} \tag{1}$$

$$\text{MOA}\ (C_{\text{Iter}}) = (\text{Min} + C_{\text{Iter}})\ ((\text{Max-Min})/M_{\text{Iter}}) \tag{2}$$

where; MOA- math optimization accelerator, C_{Iter}- current iteration, M_{Iter} - maximum iteration, Min and Max are the acceleration value selected based on the data to be optimized.

$$x_{i,j}\ (C_{\text{Iter}} + 1) = \begin{cases} \text{best}\left(x_j\right) \div (\text{MOP} + \epsilon) \times \left(\left(UB_j - LB_j\right) \times \mu + LB_j\right), & r2 < 0.5 \\ \text{best}\left(x_j\right) \times \text{MOP} \times \left(\left(UB_j - LB_j\right) \times \mu + LB_j\right), & \text{otherwise} \end{cases} \tag{3}$$

where; MOP- Math Optimizer probability, x_j- candidate solution, best $\left(x_j\right)$ - best candidate, UB_j- upper bound, LB_j- lower bound, ϵ- a small integer (0.05), $\mu = 0.5$, and r2 = r3 = random value $\epsilon\,[0, 1]$.

$$\text{MOP}\ (C_{\text{Iter}}) = 1 - \frac{{C_{\text{Iter}}}^{1/\propto}}{{M_{\text{Iter}}}^{1/\propto}} \tag{4}$$

where; $\propto = 5$

$$x_{i,j}\ (C_{\text{Iter}} + 1) = \begin{cases} \text{best}\left(x_j\right) - \text{MOP} \times \left(\left(UB_j - LB_j\right) \times \mu + LB_j\right), & r3 < 0.5 \\ \text{best}\left(x_j\right) + \text{MOP} \times \left(\left(UB_j - LB_j\right) \times \mu + LB_j\right), & \text{otherwise} \end{cases} \tag{5}$$

The above equations clearly demotes that the proposed algorithm only needs a fewer algorithm parameters and the operation can be mathematically explainable; since it uses only a basic arithmetic

operations in which the Eqn. (3) presents the exploration and Eqn. (5) shows the exploitation process. This algorithm is allowed to run till its M_{Iter} is reached to find the optimal solutions. This AA is initiated with the following initial parameters: agent size = 25, search dimension = 2, total iterations = 1500, and monitoring cost value = minimized distance among two features as shown in Eqn. (6). The required details regarding feature reduction are available in [39], and this technique aids in lowering the feature value in this study. The expression for the CD can be found in Eqn. (6), in which the 'a' and 'b' represents the data points [40];

$$\text{distance} = \sqrt{(a_1 - a_2)^2 + (b_1 - b_2)^2} \tag{6}$$

Related information on AA can be found in [37–40].

3.6 Feature Selection

This part presents the necessary detail about the feature reduction on LDLM and LBP and generation of the new FF vector using serial concatenation of the selected features. In this process, the recorded features available in .CSV format are considered for the optimization task. Based on the detection accuracy (ACC), the optimal DL scheme with decreased feature is next determined. The two optimal DL schemes (MNV1 and NNL) with the highest accuracy are then serially combined to produce the FF for additional analysis.

This work implemented 2-dimensional search using the AA by considering the maximized CD as the cost value. The proposed AA search is separately executed on the LDLM-models, like MNV1 and NNL initially. Later, similar process is executed on the LBP and the attained outcome is then combined with the chosen LDLM-features to get a new FF vector.

The initial features considered during this study are presented in Eqns. (7) to (9);

$$\text{MNV1}_{(1x1x1000} = \text{MNV1}_{(1,1)},\ \text{MNV1}_{(1,2)}, \ldots,\ \text{MNV1}_{(1,1000)} \tag{7}$$

$$\text{NNL}_{(1x1x1000)} = \text{NNL}_{(1,1)},\ \text{NNL}_{(1,2)}, \ldots,\ \text{NNL}_{(1,1000)} \tag{8}$$

$$\text{LBP}_{(1x1x236)} = \text{NNL}_{(1,1)},\ \text{NNL}_{(1,2)}, \ldots,\ \text{NNL}_{(1,236)} \tag{9}$$

The AA-optimized features are presented in Eqns. (10) to (12);

$$\text{MNV1}_{(1x1x317)} = \text{MNV1}_{(1,1)},\ \text{MNV1}_{(1,2)}, \ldots,\ \text{MNV1}_{(1,317)} \tag{10}$$

$$\text{NNL}_{(1x1x402)} = \text{NNL}_{(1,1)},\ \text{NNL}_{(1,2)}, \ldots,\ \text{NNL}_{(1,402)} \tag{11}$$

$$\text{LBP}_{(1x1x74)} = \text{NNL}_{(1,1)},\ \text{NNL}_{(1,2)}, \ldots,\ \text{NNL}_{(1,74)} \tag{12}$$

These features are serially fused to get different feature vectors as sown in Eqns. (13) to (16);

$$\text{FF1}_{(1x1x719)} = \text{MNV1}_{(1x1x317)} + \text{NNL}_{(1x1x402)} \tag{13}$$

$$\text{FF2}_{(1x1x391)} = \text{MNV1}_{(1x1x317)} + \text{LBP}_{(1x1x74)} \tag{14}$$

$$\text{FF3}_{(1x1x476)} = \text{NNL}_{(1x1x402)} + \text{LBP}_{(1x1x74)} \tag{15}$$

$$\text{FF4}_{(1x1x793)} = \text{MNV1}_{(1x1x317)} + \text{NNL}_{(1x1x402)} + \text{LBP}_{(1x1x74)} \tag{16}$$

This framework's merit is individually verified using various FF's depicted in Eqns. (13) to (16) and based on the outcome, a suitable FF is chosen. FF1 consist the combined LDLM features, FF2

and FF3 consist LDLM feature with the LBP, and FF3 includes the MNV1, NNL, and LBP features. The classification is analysed using chosen binary classifiers, like Naïve Bayes (NB), Decision Tree (DT), Random Forest (RF), K-Nearest Neighbour (KNN), and support Vector Machines (SVM). The detection accuracy with the FF4 is better compared to other FFs, hence the developed framework considered the FF4 as its feature vector.

3.7 Performance Validation

The significance of the developed framework needs to be confirmed using the chosen X-ray/CT images before it is recommended for the clinical data examination task. The developed scheme must work well in the clinical environment and it must also support the scalability. The developed framework is verified using the Python-software on a computer with an Intel i7 processor, 20 GB RAM, and 4GB VRAM. This work considered the outcome of the CM to compute metrics, like ACC, PRE, SEN, SPE, and F1S. Further, t his work also computed the Receiver Operating Characteristic (ROC) to verify the merit of the developed COVID-19 detection system for X-ray/CT images. The necessary details about the metrics chosen in this research can be found in [31].

4. RESULT AND DISCUSSIONS

This section of the research presents the experimental outcome achieved with the proposed COVID-19 detection framework from X-ray/CT images. The investigational results are separately presented for both the image cases with various FF vectors and based on the achieved outcome; the merit of this technique is verified.

Initially, MNV1-model is employed to categorize the X-ray data using SM classifier. This investigation is performed using 150 epochs and the training/validation results obtained with this process is depicted in FIGURE 5. FIGURE 5(a) depicts the accuracy and FIGURE 5(b), shows the loss for the implemented scheme. This confirms that the best training accuracy is >97% and the best validation accuracy is >94%. FIGURE 6 presents the convolution-layer (CL) outcome obtained with this model for a chosen X-ray data. FIGURE 6(a) – FIGURE 6(d) shows the outcome for CL1 to CL4. This verifies that the MNV1 helps to effectively transform the image pixels into features. The final outcome of this process after the fully-connected layer yields a feature size of 1x1x1000, which is considered to get the necessary outcome after the SM-based classification. The outcome of this process in the CM and based on the metrics of the CM, the necessary value; ROC-curve is also created and this confirms a better value with the MNV1 (0.982) as shown in FIGURE 7. FIGURE 7(a) and FIGURE 7(a)(b) shows the CM and ROC-curve attained with this task.

From the CM-values, the metrics, like ACC, PRE, SEN, SPE, and F1S are computed and these values are depicted in TABLE 4. Similar to MNV1, the classification of the chosen X-ray database is performed using other chosen LDLM and the attained results are depicted in TABLE 4. This table confirms that the MNV1 and NNL provides an improved detection accuracy compared to other models, and hence these two models are considered for the features-optimization process using the AA and then chosen to compute the FF-vectors, like FF1, FF2, FF3, and FF4. FIGURE 8 depicts

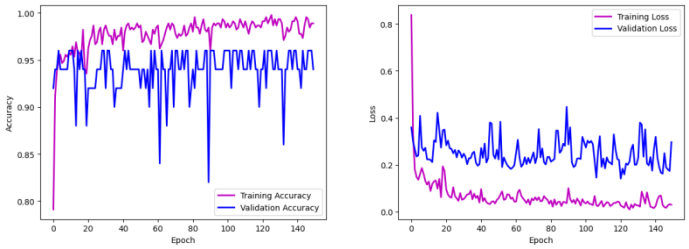

(a) Accuracy Vs epochs (b) Loss Vs Epochs

Figure 5: Performance of MNV1 and SM based detection using X-ray images

the glyph-plot for TABLE 4, metrics and this figure also graphically confirms that the MNV1 and NNL offers better overall result than other models in this study.

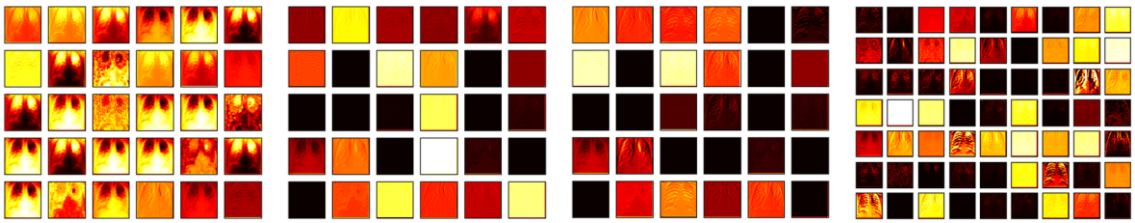

(a) CL1 (b) CL1 (c) CL1 (d) CL1

Figure 6: Processed X-ray image from the chosen CLs of MNV1

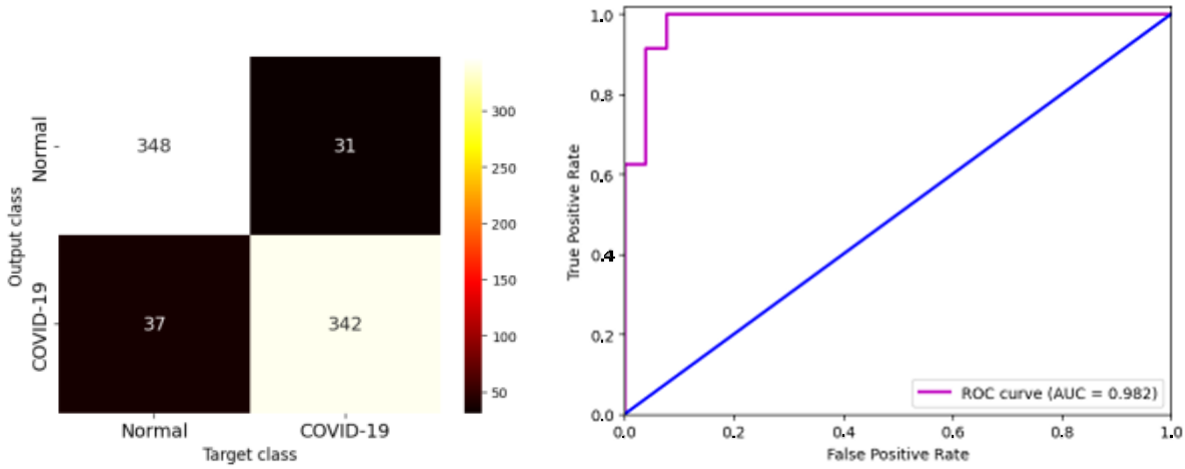

(a) CM (b) ROC-curve

Figure 7: Experimental outcome with MNV1 and SM for X-ray database

After verifying the performance of the developed framework with the X-ray database, the investigation is repeated using the CT image data. Similar to the earlier work, this work also started with the MNV1-model and the initial training results for 150 epochs is depicted in FIGURE 9. FIGURE 9(a) shows the accuracy and FIGURE 9(b), presents loss. FIGURE 9(c) shows the CM

Table 4: Initial experimental outcome with various LDLM and SM classifier for X-ray database

Model	TP	FN	TN	FP	ACC	PRE	SEN	SPE	F1S
MNV1	342	37	348	31	91.0290	91.6890	90.2375	91.8206	90.9574
MNV2	340	39	343	36	90.1055	90.4255	89.7098	90.5013	90.0662
MNV3S	331	48	344	35	89.0501	90.4372	87.3351	90.7652	88.8591
MNV3L	347	32	341	38	90.7652	90.1299	91.5567	89.9736	90.8377
NNM	342	37	343	36	90.3694	90.4762	90.2375	90.5013	90.3567
NNL	345	34	346	33	91.1609	91.2698	91.0290	91.2929	91.1493
SN	341	38	340	39	89.8417	89.7368	89.9736	89.7098	89.8551

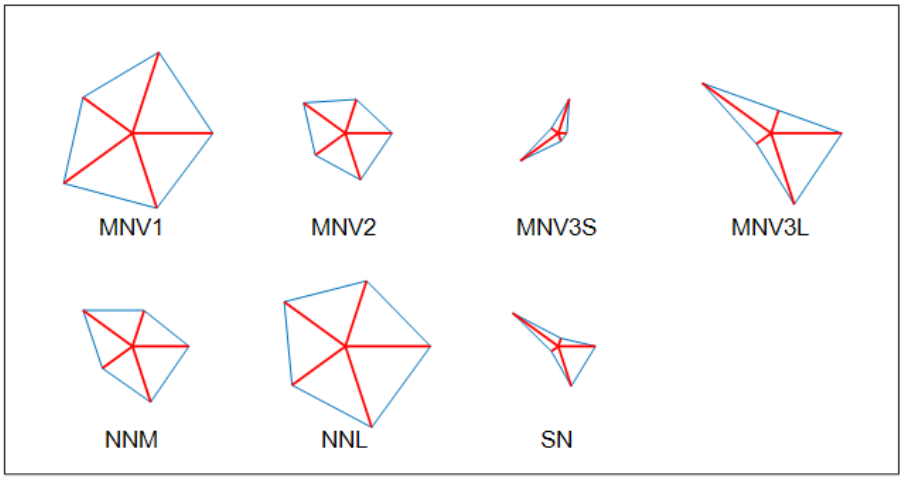

Figure 8: Overall comparison of TABLE 4 metrics using Glyph-plot

and FIGURE 9(d), depicts ROC-curve and the attained results are presented in TABLE 5. From this table, it can be confirmed that the MNV1 and NNL provides a better result for the chosen CT database. Like in X-ray database, the CT-database examination also then classified by considering the FF1, FF2, FF3, and FF4 obtained using MNV1 and NNL.

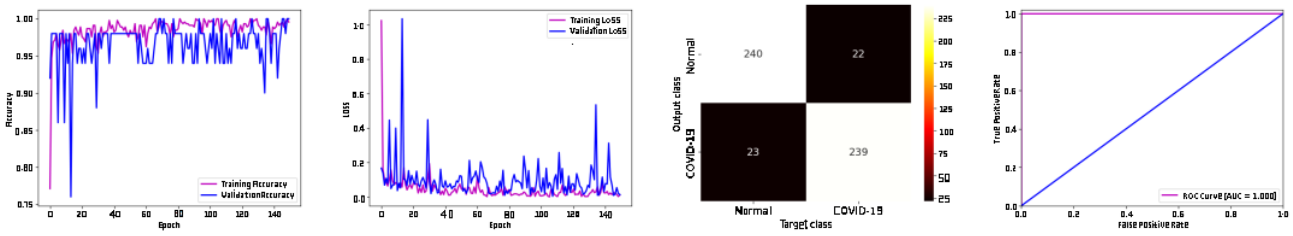

(a) Accuracy (b) Loss (c) CM (d) ROC-curve

Figure 9: Performance of MNV1 and SM based detection using CT slices

Table 5: Initial experimental outcome with various LDLM and SM classifier for CT database

Model	TP	FN	TN	FP	ACC	PRE	SEN	SPE	F1S
MNV1	239	23	240	22	91.4122	91.5709	91.2214	91.6031	91.3958
MNV2	236	26	241	21	91.0305	91.8288	90.0763	91.9847	90.9441
MNV3S	239	23	234	28	90.2672	89.5131	91.2214	89.3130	90.3592
MNV3L	240	22	235	27	90.6489	89.8876	91.6031	89.6947	90.7372
NNM	241	21	234	28	90.6489	89.5911	91.9847	89.3130	90.7721
NNL	242	20	241	21	92.1756	92.0152	92.3664	91.9847	92.1905
SN	240	22	237	25	91.0305	90.5660	91.6031	90.4580	91.0816

Verification of the developed disease detection framework is performed using various FF-vectors and the achieved results for the X-ray dataset is shown in TABLE 6. This table shows that the result of FF4 is better compared to FF1, FF2, and FF3 based results for the chosen classifiers. Further, this table also confirms that the FF4 based detection provides s superior results when KNN classifier is considered. This KNN provides an accuracy of 99.4723% which is superior compared to other ACC recorded in this table for the X-ray database.

Table 6: Experimental outcome of proposed framework for various FF on X-ray database

Features	**Model**	**TP**	**FN**	**TN**	**FP**	**ACC**	**PRE**	**SEN**	**SPE**	**F1S**
FF1	NB	362	17	364	15	95.7784	96.0212	95.5145	96.0422	95.7672
	DT	364	15	363	16	95.9103	95.7895	96.0422	95.7784	95.9157
	RF	361	18	365	14	95.7784	96.2667	95.2507	96.3061	95.7560
	KNN	367	12	366	13	96.7018	96.5789	96.8338	96.5699	96.7062
	SVM	368	11	361	18	96.1741	95.3368	97.0976	95.2507	96.2092
FF2	NB	359	20	354	25	94.0633	93.4896	94.7230	93.4037	94.1022
	DT	361	18	355	24	94.4591	93.7662	95.2507	93.6675	94.5026
	RF	360	19	357	22	94.5910	94.2408	94.9868	94.1953	94.6124
	KNN	358	21	362	17	94.9868	95.4667	94.4591	95.5145	94.9602
	SVM	360	19	359	20	94.8549	94.7368	94.9868	94.7230	94.8617
FF3	NB	361	18	367	12	96.0422	96.7828	95.2507	96.8338	96.0106
	DT	364	15	363	16	95.9103	95.7895	96.0422	95.7784	95.9157
	RF	366	13	365	14	96.4380	96.3158	96.5699	96.3061	96.4427
	KNN	365	14	369	10	96.8338	97.3333	96.3061	97.3615	96.8170
	SVM	362	17	368	11	96.3061	97.0509	95.5145	97.0976	96.2766
FF4	NB	371	8	375	4	98.4169	98.9333	97.8892	98.9446	98.4085
	DT	369	10	376	3	98.2850	99.1935	97.3615	99.2084	98.2690
	RF	373	6	374	5	98.5469	98.6772	98.4169	98.6807	98.5469
	KNN	376	3	378	1	99.4723	99.7347	99.2084	99.7361	99.4709
	SVM	377	2	375	4	99.2084	98.9501	99.4723	98.9446	99.2105

Similar task is then repeated for the CT database with the developed feature vectors; FF1 to FF4 and the attained outcome is shown in TABLE 7. This table also confirms the merit of the FF4 compared

to other FFs and the KNN-based result with FF4 outperforms other results and helps to obtain an accuracy of 99.0458%.

Table 7: Experimental outcome of proposed framework for various FF on CT database

Features	Model	TP	FN	TN	FP	ACC	PRE	SEN	SPE	F1S
FF1	NB	251	11	256	6	96.7557	97.6654	95.8015	97.7099	96.7245
	DT	252	10	254	8	96.5649	96.9231	96.1832	96.9466	96.5517
	RF	255	7	252	10	96.7557	96.2264	97.3282	96.1832	96.7742
	KNN	253	9	255	7	96.9466	97.3077	96.5649	97.3282	96.9349
	SVM	250	12	256	6	96.5649	97.6562	95.4198	97.7099	96.5251
FF2	NB	252	10	251	11	95.9924	95.8175	96.1832	95.8015	96
	DT	250	12	253	9	95.9924	96.5251	95.4198	96.5649	95.9693
	RF	255	7	249	13	96.1832	95.1493	97.3282	95.0382	96.2264
	KNN	254	8	251	11	96.3740	95.8491	96.9466	95.8015	96.3947
	SVM	248	14	254	8	95.8015	96.8750	94.6565	96.9466	95.7529
FF3	NB	251	11	254	8	96.3740	96.9112	95.8015	96.9466	96.3532
	DT	253	9	252	10	96.3740	96.1977	96.5649	96.1832	96.3810
	RF	255	7	250	12	96.3740	95.5056	97.3282	95.4198	96.4083
	KNN	250	12	257	5	96.7557	98.0392	95.4198	98.0916	96.7118
	SVM	254	8	249	13	95.9924	95.1311	96.9466	95.0382	96.0302
FF4	NB	259	3	257	5	98.4733	98.1061	98.8550	98.0916	98.4791
	DT	260	2	256	6	98.4733	97.7444	99.2366	97.7099	98.4848
	RF	255	7	259	3	98.0916	98.8372	97.3282	98.8550	98.0769
	KNN	261	1	258	4	99.0458	98.4906	99.6183	98.4733	99.0512
	SVM	257	5	261	1	98.8550	99.6124	98.0916	99.6183	98.8462

The experimental outcome of the proposed COVID-19 detection framework confirms that the detection with FF4 and KNN provides a better detection accuracy (>99%) for both X-ray and CT databases. This confirms that the proposed framework works well on the chosen image modalities and in future, it can be considered to assist the doctors during the COVID-19 detection using X-ray/CT images. Further, the chosen images in this study can be enhanced using the image thresholding techniques to improve the detection accuracy further for both X-ray/CT data.

5. CONCLUSION

The lung infection due to COVID-19 will cause severe health issue and untreated infection may lead to death. Hence, appropriate detection and treatment is essential for the individuals infected with severe COVID-19. Clinical level confirmation of this lung infection is commonly confirmed using the medical imaging schemes, like X-ray or CT and computer algorithm based examination is widely recommended for faster and accurate detection. Due to its detection performance, the DL-based methods are widely adopted in X-ray/CT examination tasks and in this work, this process is performed using the LWDL scheme. This research aims to develop a using COVID-19 detection framework which combines the AA optimized LDLM- and LBP-features. Further, this framework

recommends the usage of the FFs to attain the better result for both X-ray and CT images. In this work, the integrated feature vector developed using MNV1, NNL, and LBP (FF4) based framework confirms that this approach helps to provide a better outcome for both the image modalities when KNN-classifier is considered. The FF4 along with the KNN helps to provide a detection accuracy of >99% for the chosen image database. In the future, it can be considered to analyse the clinically collected lung images infected with the COVID-19 disease.

6. CONFLICTS OF INTEREST

The authors declare that there is no conflict of interest.

7. DATA AVAILABILITY STATEMENT

The database used in this study can be found in the literature "El-Shafai, Walid; E. Abd El-Samie, Fathi (2020), "Extensive COVID-19 X-Ray and CT Chest Images Dataset", Mendeley Data, V3, doi: 10.17632/8h65ywd2jr.3"

8. ACKNOWLEDGMENTS

The authors extend their appreciation to the deputyship for research and innovation, ministry of education in Saudi Arabia for funding this research work through the project number (IFP-2022-22).

References

[1] Omotayo O, Muonde M, Olorunsogo TO, Ogugua JO, Maduka CP. Pandemic Epidemiology: A Comprehensive Review of COVID-19 Lessons and Future Healthcare Preparedness. Int Med Sci Res J. 2024;4:89-107.

[2] Chumachenko D, Bazilevych K, Butkevych M, Meniailov I, Parfeniuk Y, et al. Methodology for Assessing the Impact of Emergencies on the Spread of Infectious Diseases. Radioelectronic Comput Syst. 2024;2024:6-26.

[3] Aljondi R, Alghamdi S. Diagnostic Value of Imaging Modalities for COVID-19: Scoping Review. J Med Internet Res. 2020;22:e19673.

[4] Bhatele KR, Jha A, Tiwari D, Bhatele M, Sharma S, et. al. COVID-19 Detection: A Systematic Review of Machine and Deep Learning-Based Approaches Utilizing Chest X-Rays and CT Scans. Cognit Comput. 2024;16:1889-1926.

[5] Costa YM, Silva Jr SA, Teixeira LO, Pereira RM, Bertolini D, Britto Jr AS, Oliveira LS, Cavalcanti GD. COVID-19 detection on chest x-ray and ct scan: A review of the top-100 most cited papers. Sensors. 2022;22:7303.

[6] Islam MS, Al Farid FJ, Shamrat FM, Islam MN, Rashid M, et al. Challenges Issues and Future Recommendations of Deep Learning Techniques for Sars-Cov-2 Detection Utilising X-Ray and CT Images: A Comprehensive Review. PeerJ Comput Sci. 2024;10:e2517.

[7] Bhattacharya S, Reddy Maddikunta PK, Pham QV, Gadekallu TR, Krishnan S SR, et al. Deep Learning and Medical Image Processing for Coronavirus (COVID-19) Pandemic: A Survey. Sustain Cities Soc. 2021;65:102589.

[8] Barragán-Montero A, Javaid U, Valdés G, Nguyen D, Desbordes P, et al. Artificial Intelligence and Machine Learning for Medical Imaging: A Technology Review. Phys Med. 2021;83:242-256.

[9] Santos MK, Ferreira Júnior JR, Wada DT, Tenório AP, Barbosa MH, et al. Artificial Intelligence, Machine Learning, Computer-Aided Diagnosis, and Radiomics: Advances in Imaging Towards to Precision Medicine. Radiol Bras. 2019;52:387-396.

[10] Saygılı A. A New Approach for Computer-Aided Detection of Coronavirus (COVID-19) From CT and X-Ray Images Using Machine Learning Methods. Appl Soft Comput. 2021;105:107323.

[11] Subramanian N, Elharrouss O, Al-Maadeed S, Chowdhury M. A Review of Deep Learning-Based Detection Methods for COVID-19. Comput Biol Med. 2022;143:105233.

[12] El-Bouzaidi YE, Abdoun O. Advances in Artificial Intelligence for Accurate and Timely Diagnosis of COVID-19: A Comprehensive Review of Medical Imaging Analysis. Sci Afr. 2023;22:e01961.

[13] Dev K, Khowaja SA, Bist AS, Saini V, Bhatia S. Triage of Potential COVID-19 Patients From Chest X-Ray Images Using Hierarchical Convolutional Networks. Neural Comput Appl. 2023;35:23861-23876.

[14] Prity FS, Nath N, Nath A, Uddin KM. Neural Network-Based Strategies for Automatically Diagnosing of COVID-19 From X-Ray Images Utilizing Different Feature Extraction Algorithms. Netw Model Anal Health Inform Bioinformatics. 2023;12:28.

[15] Heidari A, Jafari Navimipour NJ, Unal M, Toumaj S. The COVID-19 Epidemic Analysis and Diagnosis Using Deep Learning: A Systematic Literature Review and Future Directions. Comput Biol Med. 2022;141:105141.

[16] Heidari A, Navimipour NJ, Unal M. Applications of ML/Dl in the Management of Smart Cities and Societies Based on New Trends in Information Technologies: A Systematic Literature Review. Sustain Cities Soc. 2022;85:104089.

[17] Agnihotri A, Kohli N. Challenges Opportunities and Advances Related to COVID-19 Classification Based on Deep Learning. Data Sci Manag. 2023;6:98-109.

[18] Hussain E, Hasan M, Rahman MA, Lee I, Tamanna T, et al. Corodet: A Deep Learning Based Classification for COVID-19 Detection Using Chest X-Ray Images. Chaos Solitons Fractals. 2021;142:110495.

[19] Jain R, Gupta M, Taneja S, Hemanth DJ. Deep Learning Based Detection and Analysis of COVID-19 on Chest X-Ray Images. Appl Intell (Dordr). 2021;51:1690-1700.

[20] Ozturk T, Talo M, Yildirim EA, Baloglu UB, Yildirim O, et al. Automated Detection of COVID-19 Cases Using Deep Neural Networks With X-Ray Images. Comput Biol Med. 2020;121:103792.

[21] Ayalew AM, Salau AO, Tamyalew Y, Abeje BT, Woreta N. X-Ray Image-Based COVID-19 Detection Using Deep Learning. Multimedia Tool Appl. 2023;82:44507-44525.

[22] Ulutas H, Sahin ME, Karakus MO. Application of a Novel Deep Learning Technique Using CT Images for COVID-19 Diagnosis on Embedded Systems. Alex Eng J. 2023;74:345-358.

[23] Gupta K, Bajaj v. Deep Learning Models-Based Ct-Scan Image Classification for Automated Screening of COVID-19. Biomed Signal Process Control. 2023;80:104268.

[24] Arshad A, Jabeen M, Ubaid S, Raza A, Abualigah L, et al. A Novel Ensemble Method for Enhancing Internet of Things Device Security Against Botnet Attacks. Journal Decision Analytics Journal. 2023;8:100307.

[25] Duong LT, Nguyen PT, Iovino L, Flammini M. Automatic Detection of COVID-19 From Chest X-Ray and Lung Computed Tomography Images Using Deep Neural Networks and Transfer Learning. Appl Soft Comput. 2023;132:109851.

[26] Chouat I, Echtioui A, Khemakhem R, Zouch W, Ghorbel M, et al. COVID-19 Detection in CT and Cxr Images Using Deep Learning Models. Biogerontology. 2022;23:65-84.

[27] Xue X, Chinnaperumal S, Abdulsahib GM, Manyam RR, Marappan R, et al. Design and Analysis of a Deep Learning Ensemble Framework Model for the Detection of COVID-19 and Pneumonia Using Large-Scale CT Scan and X-Ray Image Datasets. Bioengineering. 2023;10:363.

[28] Mary Shyni HM, Chitra E. A Comparative Study of X-Ray and CT Images in COVID-19 Detection Using Image Processing and Deep Learning Techniques. Comput Methods Programs Biomed Update. 2022;2:100054.

[29] Maghdid HS, Asaad AT, Ghafoor KZ, Sadiq AS, Khan MK. Diagnosing COVID-19 Pneumonia From X-Ray and CT Images Using Deep Learning and Transfer Learning Algorithms. In Multimodal image exploitation and learning SPIE. 2021;11734:99-110.

[30] Appavu NK, Babu C NK, Kadry S. COVID-19 Classification in X-Ray/CT Images Using Pretrained Deep Learning Schemes. Multimedia Tool Appl. 2024;83:83157-83177.

[31] Rajinikanth V, Biju R, Mittal N, Mittal V, Askar SS, et al. COVID-19 Detection in Lung CT Slices Using Brownian-Butterfly-Algorithm Optimized Lightweight Deep Features. Heliyon. 2024;10:e27509.

[32] https://data.mendeley.com/datasets/8h65ywd2jr/3

[33] Sanida T, Dasygenis M. A Novel Lightweight CNN for Chest X-Ray-Based Lung Disease Identification on Heterogeneous Embedded System. Appl Intell. 2024;54:4756-4780.

[34] https://keras.io/api/applications/

[35] Khan MA, Rajinikanth V, Satapathy SC, Taniar D, Mohanty JR, et al. VGG19 Network Assisted Joint Segmentation and Classification of Lung Nodules in CT Images. Diagnostics. 2021;11:2208.

[36] Gudigar A, Raghavendra U, Devasia T, Nayak K, Danish SM, et al. Global Weighted Lbp Based Entropy Features for the Assessment of Pulmonary Hypertension. Pattern Recognit Lett. 2019;125:35-41.

[37] Abualigah L, Diabat A, Mirjalili S, Abd Elaziz M, Gandomi AH. The Arithmetic Optimization Algorithm. Comput Methods Appl Mech Eng. 2021;376:113609.

[38] Abualigah L, Abusaleem A, Ikotun AM, Zitar RA, Alsoud AR, et al. Arithmetic Optimization Algorithm: A Review and Analysis. In: Metaheuristic Optimization Algorithms. Elsevier. 2024:73-87.

[39] https://www.mathworks.com/matlabcentral/fileexchange/84742-the-arithmetic-optimization-algorithm-aoa

[40] Abualigah L, Elaziz MA, Yousri D, Al-qaness MA, Ewees AA, et al. Augmented Arithmetic Optimization Algorithm Using Opposite-Based Learning and Lévy Flight Distribution for Global Optimization and Data Clustering. J Intell Manuf. 2023;34:3523-3561.